Linearity and Non-linearity of Regge Trajectories for Light Non-strange Mesons: Statistical Approach

S.S. Afonin[1]

Saint Petersburg State University, St.Petersburg 199034 Russia

NRC "Kurchatov Institute" – PNPI, Gatchina 188300 Russia

Abstract

The masses of light non-strange mesons can be parameterized as a function of the radial quantum number n and the orbital angular momentum L. We perform a detailed statistical and phenomenological comparative analysis of competing Regge-like formulas evaluated against two experimental datasets consisting of an initial sample of 27 well-established benchmark states from the 2024 PDG data and an expanded sample of 85 states using a modern (L, n)-classification proposed recently. Two linear Regge models for $M^2(L, n)$ are tested: a linear dependence with different slope for L and n, $M^2(L, n) \sim an + bL$ (Model 1), and a dependence with universal slope, $M^2(L, n) \sim a(n+L)$ (Model 2). We extract full parameter sets with their corresponding 95% confidence intervals. Model selection is performed quantitatively via the Residual Sum of Squares (RSS), the adjusted RSS, the Akaike Information Criterion, and the Bayesian Information Criterion. If the sample of 27 well-established states is used, Model 2 is statistically rejected. We argue, however, that this happens due to the S-wave states ($L = 0$). If they are excluded, the difference in predictions of both models becomes statistically insignificant and the information criteria select Model 2 as a more economical one. The S-wave states can be described by this model at the cost of introducing a nonlinear correction. We find that a physically motivated correction $d/(L+1)$, that leads to the model $M^2(L, n) \sim a(n+L)+d/(L+1)$ (Model 3), results in the best fit among the three models across all criteria. We then repeat the analysis for an expanded set of 85 states, in which the relative contribution of S-wave states is much smaller, and find that Model 2 is statistically better than Model 1, thus recovering the hydrogen-like symmetry in the Regge spectrum under consideration.

1 Introduction

The physics of confinement in QCD is clearly manifested in the highly organized structure of the spectrum of light hadrons. The mass spectrum of light mesons composed of u and d quarks has long been recognized as a testing ground for models of strong interactions in the non-perturbative regime. Because a direct derivation of these masses from the fundamental QCD Lagrangian remains hindered by the non-perturbative nature of the strong coupling constant at low energies, hadron phenomenology relies heavily on effective models, dispersive methods, dualities, and other frameworks. Among these, the concept of Regge trajectories — where the square of the hadron mass scales linearly with the quantum numbers — remains a cornerstone of hadron phenomenology [1]. Originally discovered in the context of S-matrix theory [2], the linear relationship between a meson mass squared and its orbital angular

[1]E-mail: s.afonin@spbu.ru

momentum L or radial excitation number n has found strong theoretical justification in relativistic string and flux-tube models [3].

In the valence quark approximation, a light non-strange meson (u, d quark content) can be viewed as a system of two massless or nearly massless constituents connected by a color-confining flux tube with a constant string tension σ. Semiclassical quantization of a rotating relativistic string yields the famous parent Regge trajectory relation,

$$M^2 = 2\pi\sigma L + c_0, \tag{1}$$

where the orbital slope $b = 2\pi\sigma$ is universal for a given flavor sector [2]. When extended to include radial pulsations of the string, the generalized linear ansatz typically reads (a recent discussion is given in [4]),

$$M^2 = an + bL + c, \tag{2}$$

where a represents the radial slope and b denotes the orbital slope.

A long-standing debate in contemporary hadron physics centers on the structural relationship between these two slopes, known as the question of trajectory degeneracy. Some semiclassical hadron string considerations [4] and certain implementations of the AdS/QCD holographic approach [5] imply a strict universality, enforcing $a = b$ (i.e., $M^2 \propto n + L$), which implies that a single string tension dictates both spatial rotations and radial breathing modes. However, global statistical analyses of the experimental data accumulated by collaborations such as Crystal Barrel at CERN [6,7] suggest that the radial trajectories may possess a significantly steeper slope than their angular-momentum counterparts ($a > b$), indicating a breakdown of naive universal degeneracy in the light meson spectrum [8].

Furthermore, while the asymptotic linearity of Eq. (2) holds remarkably well for highly excited states ($n, L \gg 1$), systematic deviations are frequently observed in the low-lying spectrum, particularly near the ground states ($n = L = 0$). These distortions stem from short-range physical phenomena not captured by the long-range linear confinement potential. Specifically, one-gluon exchange interactions introduce a Coulomb-like attractive behavior at small distances, while chiral symmetry breaking, spin-orbit couplings, and instanton-induced forces induce state-dependent mass shifts [9,10]. To account for these low-L anomalies without destroying the successful asymptotic linearity, phenomenological models often introduce non-linear corrections.

The primary objective of this paper is to perform a detailed, data-driven comparative analysis of these competing phenomenological frameworks. Utilizing a comprehensive benchmark dataset consisting of 27 well-established experimental mass states of light non-strange mesons [11] across different (n, L) configurations, we execute high-precision least-squares regressions. We go beyond mere goodness-of-fit evaluations by extracting the full parameter sets alongside their 95% confidence intervals. Crucially, to resolve the trade-off between model accuracy and parametric complexity, we employ information-theoretic model selection criteria, namely the Akaike Information Criterion (AIC) and the Bayesian Information Criterion (BIC). After this, we add unconfirmed states from PDG [11], expanding the set to 85 states, and repeat our statistical analysis. It is important to emphasize that any analysis of this kind strongly depends on (L, n)-assignment of unconfirmed resonances. Our present analysis will be based on the modern (L, n)-classification constructed recently in [12]. The purpose of this systematic approach is to determine whether experimental data justify the inclusion of independent slopes or short-range nonlinear corrections, shedding light on the

Table 1: The modern (L, n)-classification of light non-strange mesons according to [12]. Well established states from PDG [11] are highlighted in bold.

$L \backslash n$	0	1	2	3	4
0	$\boldsymbol{\pi}$	$\boldsymbol{\pi(1300)}$	$\boldsymbol{\pi(1800)}$	$\pi(2070)$	$\pi(2360)$
	—	$\boldsymbol{\eta(1295)}$	$\boldsymbol{\eta(1760)}$	$\eta(2010)$	$\eta(2320)$
	$\boldsymbol{\rho}$	$\boldsymbol{\rho(1450)}$	$\rho(?)$	$\rho(?)$	$\rho(?)$
	$\boldsymbol{\omega}$	$\boldsymbol{\omega(1420)}$	$\omega(?)$	$\omega(?)$	$\omega(?)$
1	$\boldsymbol{a_0(1450)}$	$a_0(1710)$	$a_0(2020)$	$a_0(?)$	
	$\boldsymbol{f_0(1370)}$	$f_0(1710)$	$f_0(2020)$	$f_0(2200)$	
	$\boldsymbol{a_1(1260)}$	$\boldsymbol{a_1(1640)}$	$a_1(1930)$	$a_1(2270)$	
	$\boldsymbol{f_1(1285)}$	$f_1(?)$	$f_1(1970)$	$f_1(2310)$	
	$\boldsymbol{b_1(1235)}$	$b_1(?)$	$b_1(1960)$	$b_1(2240)$	
	$\boldsymbol{h_1(1170)}$	$h_1(?)$	$h_1(1965)$	$h_1(2215)$	
	$\boldsymbol{a_2(1320)}$	$\boldsymbol{a_2(1700)}$	$a_2(2030)$	$a_2(2175)$	
	$\boldsymbol{f_2(1270)}$	$f_2(1750)$	$f_2(2000)$	$f_2(2295)$	
2	$\boldsymbol{\rho(1700)}$	$\rho(2000)$	$\rho(2270)$		
	$\boldsymbol{\omega(1650)}$	$\omega(1960)$	$\omega(2290)$		
	$\boldsymbol{\pi_2(1670)}$	$\pi_2(2005)$	$\pi_2(2285)$		
	$\boldsymbol{\eta_2(1645)}$	$\eta_2(2030)$	$\eta_2(2250)$		
	$\rho_2(?)$	$\rho_2(1940)$	$\rho_2(2225)$		
	$\omega_2(?)$	$\omega_2(1975)$	$\omega_2(2195)$		
	$\boldsymbol{\rho_3(1690)}$	$\rho_3(1990)$	$\rho_3(?)$		
	$\boldsymbol{\omega_3(1670)}$	$\omega_3(1945)$	$\omega_3(2285)$		
3	$a_2(1990)$	$a_2(2255)$			
	$\boldsymbol{f_2(1950)}$	$f_2(2240)$			
	$a_3(2030)$	$a_3(2275)$			
	$f_3(2050)$	$f_3(2300)$			
	$b_3(2030)$	$b_3(2245)$			
	$h_3(2025)$	$h_3(2275)$			
	$\boldsymbol{a_4(1970)}$	$a_4(2255)$			
	$\boldsymbol{f_4(2050)}$	$f_4(2300)$			
4	$\rho_3(2250)$				
	$\omega_3(2255)$				
	$\pi_4(2250)$				
	$\eta_4(2330)$				
	$\rho_4(2230)$				
	$\omega_4(2250)$				
	$\rho_5(2350)$				
	$\omega_5(2250)$				

underlying dynamics of quark confinement. The results of our statistical study are presented in Conclusion.

2 Linear Regge and radial trajectories vs. experimental data on light non-strange mesons

The spectrum of light non-strange mesons used in this analysis is shown in Table 1. Their masses are given in Table 2. The pion is excluded due to its specific goldstone nature.

We will fit this spectrum using three distinct Regge-like models, each carrying a different physical interpretation:

1. **Model 1: Independent Slopes Model**

$$M^2 = an + bL + c \tag{3}$$

Here, a represents the radial Regge trajectory slope, b denotes the orbital Regge trajectory slope, and c is the intercept corresponding to the ground-state mass squared $(n = 0, L = 0)$. Physically, $a \neq b$ implies that exciting a meson radially requires a different amount of energy than increasing its spatial rotation.

Table 2: The experimental masses (in GeV) of states in Table 1 [11].

$L \backslash n$	0	1	2	3	4
0	— — $\mathbf{0.775}$ $\mathbf{0.783}$	$\mathbf{1.300 \pm 0.100}$ $\mathbf{1.294 \pm 0.004}$ $\mathbf{1.465 \pm 0.025}$ $\mathbf{1.410 \pm 0.060}$	$\mathbf{1.810 \pm 0.010}$ $\mathbf{1.751 \pm 0.015}$ — —	2.070 ± 0.035 2.010 ± 0.060 — —	2.360 ± 0.025 2.320 ± 0.015 — —
1	$\mathbf{1.439 \pm 0.034}$ $\mathbf{1.350 \pm 0.150}$ $\mathbf{1.230 \pm 0.040}$ $\mathbf{1.282 \pm 0.001}$ $\mathbf{1.230 \pm 0.003}$ $\mathbf{1.166 \pm 0.008}$ $\mathbf{1.318 \pm 0.001}$ $\mathbf{1.275 \pm 0.001}$	1.713 ± 0.019 1.733 ± 0.008 $\mathbf{1.655 \pm 0.016}$ — — — $\mathbf{1.706 \pm 0.014}$ 1.755 ± 0.010	2.025 ± 0.030 1.982 ± 0.057 1.930 ± 0.070 1.971 ± 0.015 1.960 ± 0.035 1.965 ± 0.045 2.030 ± 0.020 2.001 ± 0.010	— 2.187 ± 0.014 2.270 ± 0.055 2.310 ± 0.060 2.240 ± 0.035 2.215 ± 0.040 2.175 ± 0.040 2.293 ± 0.013	
2	$\mathbf{1.720 \pm 0.020}$ $\mathbf{1.670 \pm 0.030}$ $\mathbf{1.671 \pm 0.002}$ $\mathbf{1.617 \pm 0.005}$ — — $\mathbf{1.689 \pm 0.002}$ $\mathbf{1.667 \pm 0.004}$	2.000 ± 0.030 1.960 ± 0.025 1.963 ± 0.027 2.030 ± 0.020 1.940 ± 0.040 1.975 ± 0.020 1.982 ± 0.014 1.945 ± 0.020	2.265 ± 0.040 2.290 ± 0.020 2.285 ± 0.045 2.248 ± 0.020 2.225 ± 0.035 2.195 ± 0.030 — 2.285 ± 0.060		
3	2.050 ± 0.050 $\mathbf{1.936 \pm 0.012}$ 2.031 ± 0.012 2.048 ± 0.008 2.032 ± 0.012 2.025 ± 0.020 $\mathbf{1.967 \pm 0.016}$ $\mathbf{2.018 \pm 0.011}$	2.255 ± 0.020 2.240 ± 0.015 2.275 ± 0.035 2.334 ± 0.025 2.245 ± 0.050 2.275 ± 0.025 2.255 ± 0.040 2.283 ± 0.017			
4	2.260 ± 0.020 2.255 ± 0.015 2.250 ± 0.015 2.328 ± 0.038 2.230 ± 0.025 2.250 ± 0.030 2.330 ± 0.035 2.250 ± 0.070				

2. **Model 2: Universal Slope (Degenerate) Model**

$$M^2 = a(n + L) + c \tag{4}$$

This formulation enforces a strict constraint $a = b$. In semiclassical flux-tube or string models, a universal slope directly implies a unique, undivided string tension σ governing both radial and angular string stretching. This spectrum exhibits classical hydrogen-like degeneracy.

3. **Model 3: Non-Linear Corrected Model**

$$M^2 = a(n + L) + \frac{d}{L + 1} + c \tag{5}$$

This ansatz re-introduces the universal slope a for large excitations but adds a non-linear term governed by parameter d. The factor $d/(L+1)$ acts as a short-range or spin-orbit correction. As $L \to \infty$, this term vanishes, recovering the asymptotic linearity. A positive d signifies an extra attractive contribution at low orbital momentum. The form of this correction is motivated by the first relativistic correction to the hydrogen-like spectrum (i.e. depending only on the principal quantum number $n + L + 1$) of the Dirac particle in the Coulomb field [13].

3 Global analysis

As Table 2 shows, experimental uncertainties in meson mass determinations can vary by two orders of magnitude. In this situation, the standard χ^2 method will yield unreliable results and will require modification. This task is deferred to a future study. We will conduct a statistical analysis using the least-squares method for the central values.

First we consider subset containing 27 experimental points corresponding to well established states in Table 2. Then the whole set of 85 experimental states from Table 2 is analyzed.

We implement multiple robust metrics to contrast the performance of these models across two separate datasets containing 27 and 85 experimental points respectively. The Residual Sum of Squares (RSS) measures the total unexplained variance within the experimental dataset. The adjusted coefficient of determination (R^2_{adj}) penalizes the standard R^2 value based on the number of predictors. To resolve the trade-off between model accuracy and parametric complexity, we employ information-theoretic model selection criteria. The Akaike Information Criterion ($\text{AIC} = N \ln(\text{RSS}/N) + 2k$) estimates information loss while penalizing the number of free parameters (k) to prevent overfitting. The Bayesian Information Criterion ($\text{BIC} = N \ln(\text{RSS}/N) + k \ln(N)$) introduces a stricter complexity penalty based on the total sample size (N).

The results are summarized in Table 3.

Table 3: Extracted parameter values, 95% confidence intervals (CI), and comprehensive goodness-of-fit metrics for the initial ($N = 27$) and extended ($N = 85$) meson datasets.

Dataset & Model	**Parameter**	**Value ± Error / [95% CI]**	**RSS**	R^2_{adj}	**AIC**	**BIC**
Initial Dataset ($N = 27$)						
Model 1: $an + bL + c$	a	1.275 ± 0.066 $[1.140, 1.410]$	0.6961	0.9651	-16.146	-12.259
	b	1.100 ± 0.042 $[1.014, 1.186]$				
	c	0.579 ± 0.073 $[0.428, 0.729]$				
Model 2: $a(n + L) + c$	a	1.108 ± 0.049 $[1.007, 1.209]$	1.0100	0.9513	-8.095	-5.503
	c	0.631 ± 0.084 $[0.457, 0.804]$				
Model 3: $a(n + L) + \frac{d}{L+1} + c$	a	1.215 ± 0.052	**0.6850**	**0.9678**	**-16.578**	**-12.691**
	d	0.488 ± 0.038				
	c	0.183 ± 0.041				
Extended Dataset ($N = 85$)						
Model 1: $an + bL + c$	a	1.139 ± 0.043 $[1.096, 1.182]$	2.7749	0.9795	-284.87	-277.55
	b	1.120 ± 0.039 $[1.081, 1.159]$				
	c	0.616 ± 0.110 $[0.506, 0.726]$				
Model 2: $a(n + L) + c$	a	1.128 ± 0.035 $[1.093, 1.163]$	2.8082	0.9795	**-285.86**	**-280.97**
	c	0.614 ± 0.109 $[0.505, 0.723]$				

An examination of the empirical results reveals a clear evolution of the trajectory dynamics depending on the dataset scale. For the initial 27-point dataset, Model 2 yields the poorest performance across all metrics, generating the highest RSS (1.0100) and the lowest R^2_{adj} (0.9513). Model 1 shows a noticeable improvement, extracting a radial slope ($a = 1.275\,\text{GeV}^2$) that is 16% larger than the orbital slope ($b = 1.100\,\text{GeV}^2$). Because their respective 95% confidence intervals show minimal overlap, a standard nested F-test strongly rejects the null hypothesis of pure linear degeneracy ($a = b$) for this smaller sample, yielding a p-value of 0.0031. However, Model 3 emerges as the mathematically superior framework for these 27 states, achieving the absolute minimum residual variance ($\text{RSS} = 0.6850$) and the lowest information loss ($\text{AIC} = -16.578$, $\text{BIC} = -12.691$). The extracted positive value of $d = 0.488$ successfully models the empirical lifting of masses near the ground states caused by short-range physics.

Crucially, a dramatic shift occurs when the sample size is expanded to the 85-point extended dataset by including higher orbital angular momenta ($L = 3, 4$). In this wider energy regime, the extracted independent slopes in Model 1 immediately converge, yielding $a = 1.139, \mathrm{GeV}^2$ and $b = 1.120, \mathrm{GeV}^2$. The 95% confidence intervals for these two slopes now exhibit a substantial and dominant overlap ($(1.096, 1.182)$ versus $(1.081, 1.159)$).

Performing the nested F-test on the extended data set yields an F-statistic of 0.985 with a corresponding p-value of 0.324 that is significantly greater than the standard 0.05 threshold below which the hypothesis of trajectory degeneracy ($a = b$) must be rejected. In more detail, the null hypothesis states that the two slopes are equal ($H_0 : a = b$). The test statistic is calculated as follows,

$$F = \frac{(\mathrm{RSS}_2 - \mathrm{RSS}_1)/(k_1 - k_2)}{\mathrm{RSS}_1/(N - k_1)} = \frac{(2.8082 - 2.7749)/1}{2.7749/(85 - 3)} = 0.985. \tag{6}$$

Since $p = 0.324 > 0.05$, we fail to reject the null hypothesis H_0. The difference between parameters a and b is statistically insignificant.

This convergence of slopes is robustly confirmed by the information criteria. The adjusted coefficient of determination for both Model 1 and Model 2 becomes completely identical at 0.9795. According to Occam's razor, because the additional parameter in Model 1 fails to deliver any statistically meaningful reduction in the residual variance, the simpler model is mathematically preferred. Model 2 successfully minimizes the information metrics, yielding a lower AIC (-285.86 versus -284.87) and a significantly lower BIC (-280.97 versus -277.55). A difference of $\Delta\mathrm{BIC} = 3.42$ provides positive statistical evidence in favor of the degenerate linear formulation.

Graphically, the Regge trajectories of both models differ little; for the second model, they are presented in Fig. 1. This demonstrates that as higher-lying states are factored into the regression, the relative impact of low-L short-range anomalies diminishes, and the universal linear trajectory rule predicted by semiclassical string tension effectively governs the global meson spectrum. To obtain this conclusion, the non-linear correction is no longer required, so Model 3 was omitted in Table 3 for the extended dataset.

4 Analysis with excluded S-wave states

If we restrict ourselves to the well-known non-strange mesons from PDG, the inequality of slopes of the orbital and radial trajectory would seem obvious. However, a closer look at the experimental masses in Table 2 reveals that the main contribution to this inequality comes from states with $L = 0$. This suggests that there are two possibilities for preserving the equality of slopes: (1) introducing a nonlinear correction in L; (2) excluding S-wave states from the fit. Model 3 was intentionally introduced above to demonstrate the first possibility using a specific example. In this section, we demonstrate the second possibility.

Separating out the states with $L = 0$ in Table 2 leaves a set of 19 well-established mesons and 73 states in the extended dataset. In the first case, the results are given in Table 4.

An F-test was conducted to verify whether adding the independent parameter b significantly improves the fit quality. The test yields an F-statistic of 0.0887, corresponding to a p-value of 0.7697. Since $p > 0.05$, we fail to reject the null hypothesis that $a = b$. This means that in Model 1, the calculated slopes along the n axis ($a = 1.160$) and the L axis

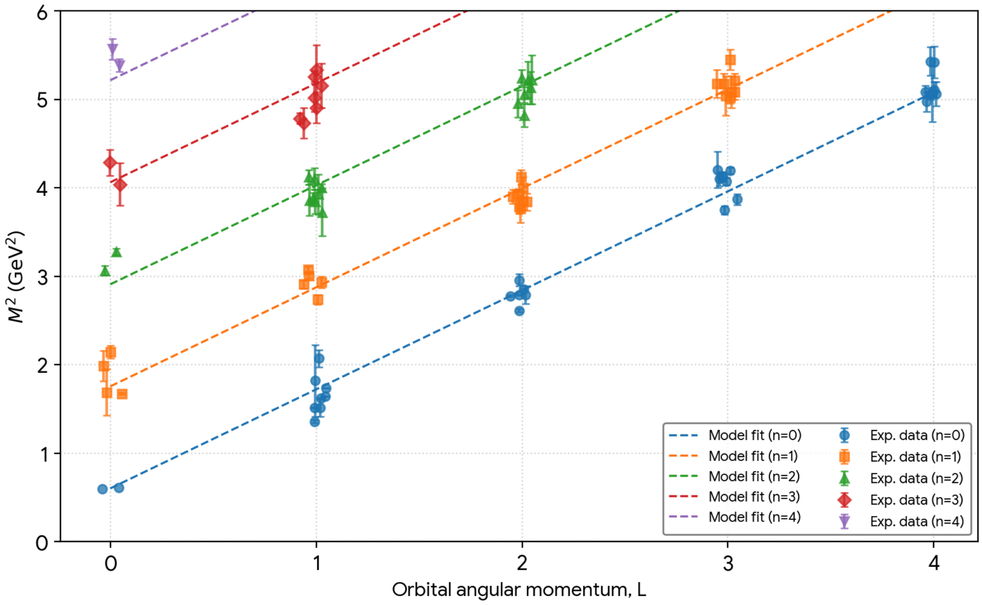

Figure 1: Regge trajectories for the linear fit using all 85 experimental points.

Table 4: Fitting results for the 19-point dataset ($L > 0$).

Parameter / Metric	**Model 1**	**Model 2**
Parameter a	1.160 ± 0.284	1.124 ± 0.113
Parameter b	1.122 ± 0.118	—
Parameter c	0.543 ± 0.219	0.544 ± 0.212
Residual Sum of Squares (RSS)	0.4685	0.4711
Residual Standard Error (RSE)	0.1711	0.1665
Degrees of Freedom (dof)	16	17

($b = 1.122$) are statistically indistinguishable within their respective error margins. Model 2 yields a lower Residual Standard Error ($RSE = 0.1665$) because eliminating the redundant parameter increases the degrees of freedom without causing a substantial increase in RSS. Thus, *Model 2 is statistically preferred.*

Our analysis extended to an expanded dataset containing 73 experimental points with $L > 0$ (excluding 12 points where $L = 0$) is summarized in Table 5.

Comparing the two models for the 73-point sample via F-test for nested models yields an F-statistic of 3.445, which results in a p-value of 0.0677. At the standard 5% significance level ($\alpha = 0.05$), since $p > 0.05$, the null hypothesis $a = b$ *cannot be rejected.* The confidence intervals for the distinct slopes in Model 1 ($a = 1.121 \pm 0.045$ and $b = 1.162 \pm 0.044$) exhibit a substantial overlap. Thus Model 2 remains statistically superior due to its simplicity, successfully capturing the underlying physical law with fewer parameters. This strongly validates the hypothesis of a universal slope for Regge trajectories across both quantum numbers n and L. Finally the most economical and statistically preferred parametrization

Table 5: Fitting results for the expanded 73-point dataset ($L > 0$).

Parameter / Metric	**Model 1**	**Model 2**
Parameter a	1.121 ± 0.045	1.142 ± 0.039
Parameter b	1.162 ± 0.044	—
Parameter c	0.522 ± 0.126	0.542 ± 0.126
Residual Sum of Squares (RSS)	1.9322	2.0273
Residual Standard Error (RSE)	0.1661	0.1690
Degrees of Freedom (dof)	70	71

of spectrum with excluded S-wave states is (see Table 5)

$$M^2 = 1.142(n + L) + 0.542 \tag{7}$$

The obtained fit (7) is visualized in Fig. 2. An examination of the 12 excluded points with $L = 0$ reveals a systematic upward shift relative to the main regression line. This reflects known hadronic physics phenomena, where ground-state light mesons ($L = 0$) are affected by chiral symmetry breaking and non-linear radiative corrections, justifying their omission from the universal linear fit. These effects are most pronounced in the case of the pion, Fig. 2 shows that these effects contribute to masses of many S-wave mesons.

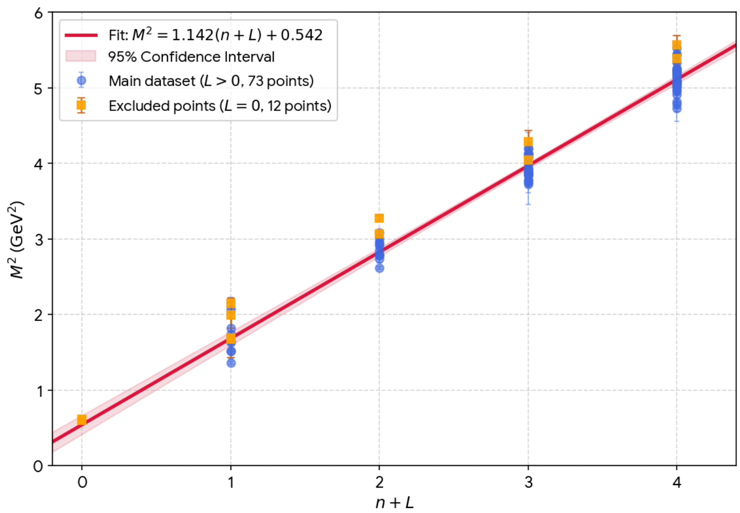

Figure 2: Global fit using the main dataset with excluded S-wave states.

Alternatively, the spectrum can be visualized as a family of parallel lines plotted against the orbital angular momentum L — the main trajectory ($n = 0$) and daughter trajectories ($n = 1, 2, 3, 4$) configured as parallel lines shifted upwards by a constant vertical step $\Delta M^2 = a \approx 1.142$ GeV^2 for each successive value of n. The corresponding plot is given in Fig. 3. The systematic upward shift of masses at $L = 0$ is clearly seen.

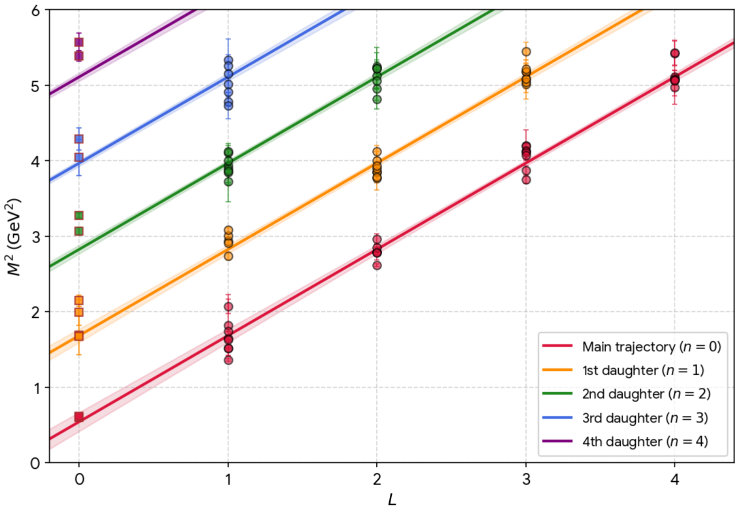

Figure 3: Regge trajectories for the linear fit using the main dataset with excluded S-wave states.

5 Conclusion

Making use of several information criteria we have performed a statistical analysis of competing Regge-like formulas describing the spectrum of light non-strange mesons — with different slope for orbital and radial trajectory and with universal slope. In the case of well-established states from PDG, the slopes are clearly different. We argued, however, that this difference can be an effective difference that emerges because non-linear corrections were not taken into account. They are important for description of the spectrum of S-wave states. This suggestion was demonstrated by a simple model with nonlinear correction of the form $M^2(L,n) \sim a(n+L) + d/(L+1)$, which has the same number of parameters as the model with different slopes, but turns out to be statistically and phenomenologically better. After that we repeated our analysis using the recently constructed (L,n)-classification of light non-strange mesons that includes 85 states [12]. It was found that the difference between two Regge models becomes statistically negligible — the degenerate linear model, $M^2 = a(n+L) + c$, successfully captures the underlying physical law with fewer degrees of freedom, strongly validating the hypothesis of a universal string tension in the global spectrum of light non-strange mesons. Thus our results confirm that the light meson spectrum is dominated by Regge behavior with universal slopes for angular and radial excitations.

References

[1] F. Gross, E. Klempt, S. J. Brodsky, A. J. Buras, V. D. Burkert, G. Heinrich, K. Jakobs, C. A. Meyer, K. Orginos and M. Strickland, *et al.* “50 Years of Quantum Chromodynamics,” Eur. Phys. J. C **83** (2023) 1125.

[2] P. D. B. Collins, *An Introduction to Regge Theory and High Energy Physics*, Cambridge University Press, 1977.

[3] Y. Nambu, “Strings, monopoles, and gauge fields,” Phys. Rev. D **10** (1974) 4262.

[4] S. Afonin and A. Tsymbal, "Dynamical $O(4)$-Symmetry in the Light Meson Spectrum within the Framework of the Regge Approach," Phys. Atom. Nucl. **87** (2024) no.Suppl 3, S477.

[5] A. Karch, E. Katz, D. T. Son, and M. A. Stephanov, "Linear confinement and AdS/QCD," Phys. Rev. D **74** (2006) 015005.

[6] A. V. Anisovich, V. V. Anisovich, and A. V. Sarantsev, "Systematics of $q\bar{q}$ states in the (n, M^2) and (J, M^2) planes," Phys. Rev. D **62** (2000) 051502.

[7] D. V. Bugg, "Four sorts of meson," Phys. Rep. **397** (2004) 257.

[8] P. Masjuan, E. Ruiz Arriola and W. Broniowski, "Systematics of radial and angular-momentum Regge trajectories of light non-strange $q\bar{q}$-states," Phys. Rev. D **85** (2012) 094006.

[9] D. Ebert, R. N. Faustov, and V. O. Galkin, "Mass spectra and Regge trajectories of light mesons in the relativistic quark model," Phys. Rev. D **79** (2009) 114029.

[10] M. Shifman and A. Vainshtein, "Highly excited hadrons, sliding states, and area law for Wilson loops," Phys. Rev. D **77** (2008) 034002.

[11] S. Navas *et al.* (Particle Data Group), Phys. Rev. D **110** (2024) 030001.

[12] S. S. Afonin, A. V. Sarantsev and A. M. Tsymbal, "Hydrogen-Like Symmetry in Regge Spectrum of Light Mesons: Selection of States," Phys. Part. Nucl. **57** (2026) no.3, 343.

[13] W. Greiner, *Relativistic Quantum Mechanics: Wave Equations*, Springer-Verlag, Berlin (2000).